

Visualization of the conductive channel in a planar resistance switching device based on electrochromic materials

Da Shan Shang, Lei Shi, Ji-Rong Sun, and Bao-Gen Shen

Citation: *J. Appl. Phys.* **111**, 053504 (2012); doi: 10.1063/1.3691204

View online: <http://dx.doi.org/10.1063/1.3691204>

View Table of Contents: <http://jap.aip.org/resource/1/JAPIAU/v111/i5>

Published by the [American Institute of Physics](#).

Related Articles

Realization of ohmic-like contact between ferromagnet and rubrene single crystal

Appl. Phys. Lett. **101**, 073501 (2012)

Multipactor saturation in parallel-plate waveguides

Phys. Plasmas **19**, 072304 (2012)

Experimental isolation of degradation mechanisms in capacitive microelectromechanical switches

Appl. Phys. Lett. **100**, 233505 (2012)

Annealed InGaN green light-emitting diodes with graphene transparent conductive electrodes

J. Appl. Phys. **111**, 114501 (2012)

Glass polarization induced drift in microelectromechanical capacitor

J. Appl. Phys. **111**, 103523 (2012)

Additional information on J. Appl. Phys.

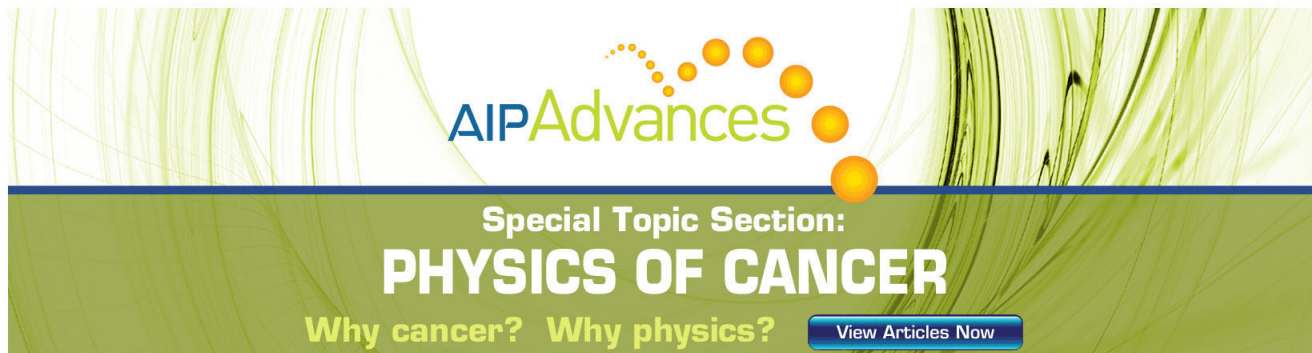
Journal Homepage: <http://jap.aip.org/>

Journal Information: http://jap.aip.org/about/about_the_journal

Top downloads: http://jap.aip.org/features/most_downloaded

Information for Authors: <http://jap.aip.org/authors>

ADVERTISEMENT



AIP Advances

Special Topic Section:
PHYSICS OF CANCER

Why cancer? Why physics? [View Articles Now](#)

Visualization of the conductive channel in a planar resistance switching device based on electrochromic materials

Da Shan Shang (尚大山,^{a)} Lei Shi (史磊), Ji-Rong Sun (孙继荣), and Bao-Gen Shen (沈保根)
Beijing National Laboratory for Condensed Matter Physics and Institute of Physics, Chinese Academy of Sciences, Beijing 100190, People's Republic of China

(Received 20 December 2011; accepted 30 January 2012; published online 2 March 2012)

In this work, bipolar resistance switching behavior was realized in an **Au/tungsten oxide/Au** planar device, and the evolution of the conductive channel during resistance switching was successfully visualized by the *in situ* optical image technique based on the color-conductivity dependence of tungsten oxide. We found that there are two types of conductive channel, named **parabolic channel** and **bar-like channel**, exist in the planar device. The parabolic channel formed firstly near the cathode and then extended to but could not touch the anode. By applying opposite electric-field, the bar-like channel formed from the cathode (i.e., foregoing anode) and extended to the parabolic channel. With alternating the external electric-field polarity, the bar-like channel showed an indirect connection and nonmonotonic disconnection with the parabolic channel at the region near the foregoing anode, corresponding to the high-to-low and low-to-high resistance switching processes of the planar device, respectively. The instable RS behavior was caused by the change of bar-like channel occurring position under the high external field condition. The conductive channel formation was ascribed to the sodium ion immersion from the soda-lime glass substrate into the tungsten oxide film and then migration driven by the electric field to form sodium tungsten bronze. These results will give some insight into the resistance switching property improvement and mechanism elucidation as well as a possibility to develop electric/optical-coupled switch and data storage devices. © 2012 American Institute of Physics. [<http://dx.doi.org/10.1063/1.3691204>]

I. INTRODUCTION

Driven by an increasing demand for portable and mobile electronic devices, the requirement for memory devices with improved functionality is rapidly growing and a variety of alternative concepts for nonvolatile memory have been proposed in the last decades.^{1,2} Electric-field-induced resistance switching (RS) effect means the material or device resistance can be changed by applying electric-field and the obtained resistance states can be maintained for a long time after removing the external field. This physical phenomenon can be traced back to 50 years ago,^{3,4} and has been refined since 2000, when a nonvolatile memory, called resistance random access memory (RRAM), was introduced.⁵ Based on the RS effect, RRAM has some advantages, such as easy fabrication, high write/read speed, low energy consumption, multi-level memory, and high scalability. Driven by these attractive potentials, a large variety of materials, including perovskite oxide,⁶ binary transition-metal oxides,⁷ and solid electrolytes,⁸ have been demonstrated to have the RS function and then have the possibility to be the candidates for RRAM fabrication. Recently, not limited to the memory, the RS phenomenon has been successfully identified as memristive systems,⁹ and then proposed in a broader range of application including the Boolean logic implementation and neuromorphic systems.^{10,11} The major roadblock to commercialize the RS-related devices is the RS physical mechanism, which is still not comprehended exactly although most of the

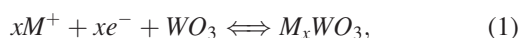
reported RS phenomena have been demonstrated to be universally relevant to redox reactions and nano-ionic transport processes.^{12,13}

From the viewpoint of RS location, a widely agreement is that the RS occurs not in the whole device but in a very local region, where conductive channels formed, and the RS is due to the reversible connection and disconnection of the conductive channels.^{14,15} In previous studies, the focus of the conductive channel investigation is mainly on the composition and structure analysis. Some methods have been used including conductive atomic force microscopy,^{14,15} X-ray adsorption spectroscopy,¹⁶ scanning electron microscope,¹⁷ photo-emission electron microscopy,¹⁸ scanning transmission electron microscope,¹⁹ and high resolution transmission electron microscope equipped with scanning tunnel microscope.²⁰ These experimental results demonstrated that the conductive channel formation should be originated from the cation (e.g., Cu⁺ and Ag⁺) or anion (e.g., O²⁻) migration driven by the electric field. However, the detailed connection/disconnection evolution processes are still unclear. For example, what happens at the moment when the connection/disconnection occurs; where the connection/disconnection occurs; why the connection/disconnection shows bipolar RS behavior especially for the channels formed by electroneutral metals, such as Cu and Ag; which factors causes the instability of connection/disconnection. Addressing these questions will be helpful to give some insights into the mechanism interpretation as well as the improvement of RS-related device performance. However, one of the main difficulties to clarify these questions is

^{a)}Electronic mail: shangdashan@iphy.ac.cn.

how to realize an *in situ* monitor of the whole evolution process of the whole conductive channel during the RS process in view of the small size and the random occurrence of the conductive channel in previous experiments. Recently, Azumi *et al.*²¹ directly observed the change of conductive regions in perovskite ferrite by means of the microspectroscopic image technique. Although the detailed connection/disconnection processes of conductive channels are still obscure in this experiment, the image technique should be an effective way for the investigation of the dynamic evolution process of conductive channels in solid electrolyte materials, since it could not only achieve the *in situ* observation but also reflect the conductive change in the whole region of the device conveniently.

Tungsten oxide (WO_{3-x}) is one of the most important electrochromic materials, and has been investigated widely for “smart windows.”²² The electrochromic process is usually described in terms of the **double-charge-injection model**, which can be written, in a simplified form, as



where $\text{M} = \text{H}^+, \text{Li}^+, \text{Na}^+$ with lower cation radius. When a M^+ (for example, Na^+) was injected into the material, together with an electron, **the valence of tungsten ion will be decreased, causing a optical change of the material from transparent to black and then to dark blue.**^{22,23} Correspondingly, the conductivity of tungsten oxide will experience a low-to-high change. As the conductivity changed locally in the materials, the color-conductivity dependence enables us to visualize the geometrical shape of regions with higher conductivity, namely conductive channel, using optical image technique. Its visibility provides a tool for gaining insight into the evolution of the conductive channel during the RS process.

In this work, we will report on a direct optical imaging technique to spatially resolve the conductive channel in a planar RS device based on WO_{3-x} film. The whole evolution processes of the conductive channel formation, connection, and disconnection during both the stable and instable RS were visualized through a change of color that accompanies the valence change of tungsten ions. In the end, we will provide the experimental evidence to discuss the origin of the conductive channels.

II. EXPERIMENT

A planar-type device was used as illustrated in Fig. 1(a). Commercial **soda-lime glasses slide** were used as a substrate. WO_{3-x} films were deposited by pulsed laser deposition using a KrF excimer laser ($\lambda = 248 \text{ nm}$) with a repetition rate of 1–5 Hz and a fluence of 5 J/cm^2 . During the deposition, the substrate temperature was maintained at $400 \text{ }^\circ\text{C}$ and the oxygen pressure was kept at 10 Pa. The thickness of the films was $\sim 400 \text{ nm}$. A tungsten oxide ceramic with the nominal composition of WO_3 was used as the target. Gold electrodes were deposited on the top of the WO_{3-x} film by DC sputtering. The size of the gold electrodes is $200 \times 200 \text{ } \mu\text{m}^2$ with an interval of $300 \text{ } \mu\text{m}$, defined by the photolithography and lift-

off technique (Fig. 1(a)). Electric property measurements were performed using a Keithley 2601 sourcemeter under air and vacuum ($< 1 \times 10^{-5} \text{ Torr}$). Two gold probes were contacted to the gold electrodes for the electric field applying and resistance measurement. Simultaneously, the spatially resolved color change of the sample was measured by illuminating it with light emitted from halogen light sources (China, MORITEX MHAA-100 W) with a light output of 400–700 nm. The images were recorded by a computer-controlled complementary metal oxide semiconductor (CMOS) camera (Japan, ARTRAY-130MI) with a microscope lens. The surface morphology and elementary composition of the film were measured by scanning electron microscope (SEM) (Japan, JEOLS-4800) and energy dispersive spectroscopy (EDS) (USA, EDAX-Genesis), respectively. Raman spectra were recorded in back-scattering configuration using a confocal micro-Raman spectrometer (France, Horiba/Jobin Yvon HR800) with a 532 nm laser line used as the excitation source. The laser beam was focused using a $50 \times$ objective with numeric aperture $\text{NA} = 0.5$, and the spot size of the laser beam is about $1.5 \text{ } \mu\text{m}$.

III. RESULTS AND DISCUSSION

Figure 1(b) shows the current-voltage (*I-V*) characteristics of the sample. Under the voltage range from -30 V to 30 V , the *I-V* curve shows a good linear feature, indicating a good ohmic contact between the gold electrodes and the film (inset in Fig. 1(b)). With increasing the applied voltage to 80 V , an obvious *I-V* hysteresis appeared. The *I-V* hysteresis is usually considered as a typical feature of the RS phenomenon, indicating that the device resistance has changed during the voltage sweeping. Meanwhile, from the photo image, a dark-color region with a parabolic shape grown up from the cathode toward the anode was observed (up-side of Fig. 1(c)). A direct probe measurement showed a higher conductivity ($\sim 1.1 \times 10^{-4} \text{ S/cm}$) in the dark-colored region than elsewhere ($\sim 1.5 \times 10^{-5} \text{ S/cm}$). Therefore, the dark-colored region was considered as the conductive channel, which played a dominant role of decreasing the sample resistance between the two gold electrodes. Different from the previous reported results where the conductive channel usually was assumed to penetrate through the material.^{12–20} However, the conductive channel cannot touch the anode even though we continue increasing the applied voltage. Under a higher voltage condition, a breakdown-like behavior of the film occurred. We can see a filament region appeared abruptly between the vaulted top of the parabolic channel and the anode (down-side of Fig. 1(c)). From the SEM image, it can be seen that the breakdown caused some dendritic-like phases precipitated from the film, as shown in Fig. 1(d). Once the phase precipitation occurs, it cannot be removed and will spoil the following RS processes.

In order to avoid the breakdown-like behavior, we used a constant current mode to trigger the sample. In this case, the device voltage will decrease once the device resistance decreased, and then the breakdown-like behavior can be repressed effectively. The device resistance can be calculated from the measured voltage value divided by the

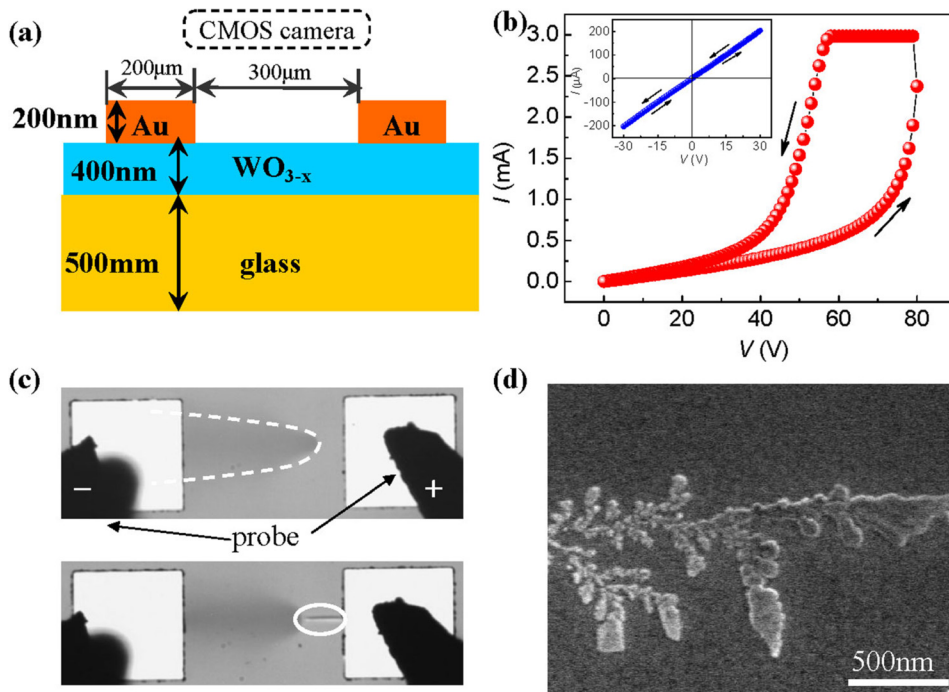


FIG. 1. (Color online) (a) Schematic of the Au/WO_{3-x}/Au planar device structure. (b) I-V curves of the planar device measured at the range from 0 to 80 V. The inset shows the IV curves measured at the range from -30 V to 30 V. (c) Up-side: photo image snapped after the voltage sweep from 0 to 80 V. Down-side: photo image snapped after permanent breakdown occurring. (d) SEM image of the breakdown region circled in the down-side image of (c).

applying constant current and should have the same variation trend as the measured voltage. The detailed processes of the conductive channel evolution with time are shown in Fig. 2. For clarity, the color change due to the conductive channel was magnified digitally by subtracting the image of the non-conductive channel region from the image and then colored. We found that the sample resistance was dominated not only by the applied current intensity but also by the current application time. Under the constant current of 3 mA, the measured voltage decreased gradually with time, indicating the device resistance decreased (Fig. 2(a)). Correspondingly, the conductive channel with a parabolic shape appeared at the left half of the planar device firstly, and then grew up from the left electrode (cathode) toward the right one (anode) with the top of the parabolic channel becoming deeper and sharper gradually (up-side of Fig. 2(d)). This process is identical to that using external voltage mode (up-side of Fig. 1(c)). Similarly, the parabolic channel cannot touch the anode even if increasing the application time. However, no filament region occurred with increasing time. When we reversed the applied current polarity, the measured voltage firstly decreased and then increased again (Fig. 2(b)). From the photo images, it can be seen that the measured voltage increasing corresponded to a deep bar-like channel protruding from the right electrode (i.e., cathode in this case), and then was pushed into the left parabolic channel (see No. 6-7 images in Fig. 2(d)). The bar-like shape of the channel should be originated from the concentration of electric-field on the position of the vaulted top of parabolic channel due to the parabolic channel formation. It should be noted that the bar-like channel differs from the filament in Fig. 1(c). The filament formed under the external bias with the same field polarity of the parabolic channel, while the bar-like channel formed with opposite field polarity to the parabolic channel.

Moreover, it can be seen that the bar-like channel grew from right electrode to left electrode (see Movie S1 in the supplementary materials²⁹), while the filament formed abruptly so that the growth direction cannot be distinguished using present apparatus. With time increasing, the bar-like channel grew toward the left electrode (i.e., anode in this case) gradually. Meanwhile, the parabolic channel disappeared and the region near the left electrode became light (see No. 8–10 images in Fig. 2(d)). This process corresponds to the measured voltage decreasing. When we reversed the current polarity again, the bar-like channel recurred at the left electrode (i.e., cathode in this case) and gradually grew toward the right electrode (i.e., anode in this case) like the former process (see No. 11–15 images in Fig. 2(d)). Correspondingly, the measured voltage also decreased initially and then increased again (Fig. 2(c)). By examining the above processes, we believe that bipolar RS behavior can be realized if we control the channel changed only between images Nos. 6 and 15.

By carefully adjusting the applying current and its application time, the bipolar RS with good stability and reproducibility was achieved, as shown in Fig. 3(a). The corresponding photo images are shown in Fig. 3(b). It can be seen clearly that, during the high-to-low RS, a bar-like channel (arrowed in the inset of Fig. 3(b)) protruded from the right side electrode and connected with the left parabolic channel, while the bar-like channel disappeared resulting in the whole conductive channel disconnection during the low-to-high RS. The disconnection and reconnection of the conductive channel only need to occur at the region near one of the electrodes, which depends on the position of parabolic channel. If the parabolic channel was formed initially at the right side electrode, the resistance switching polarity can be reversed (see Fig. S1 in the supplementary materials²⁹).

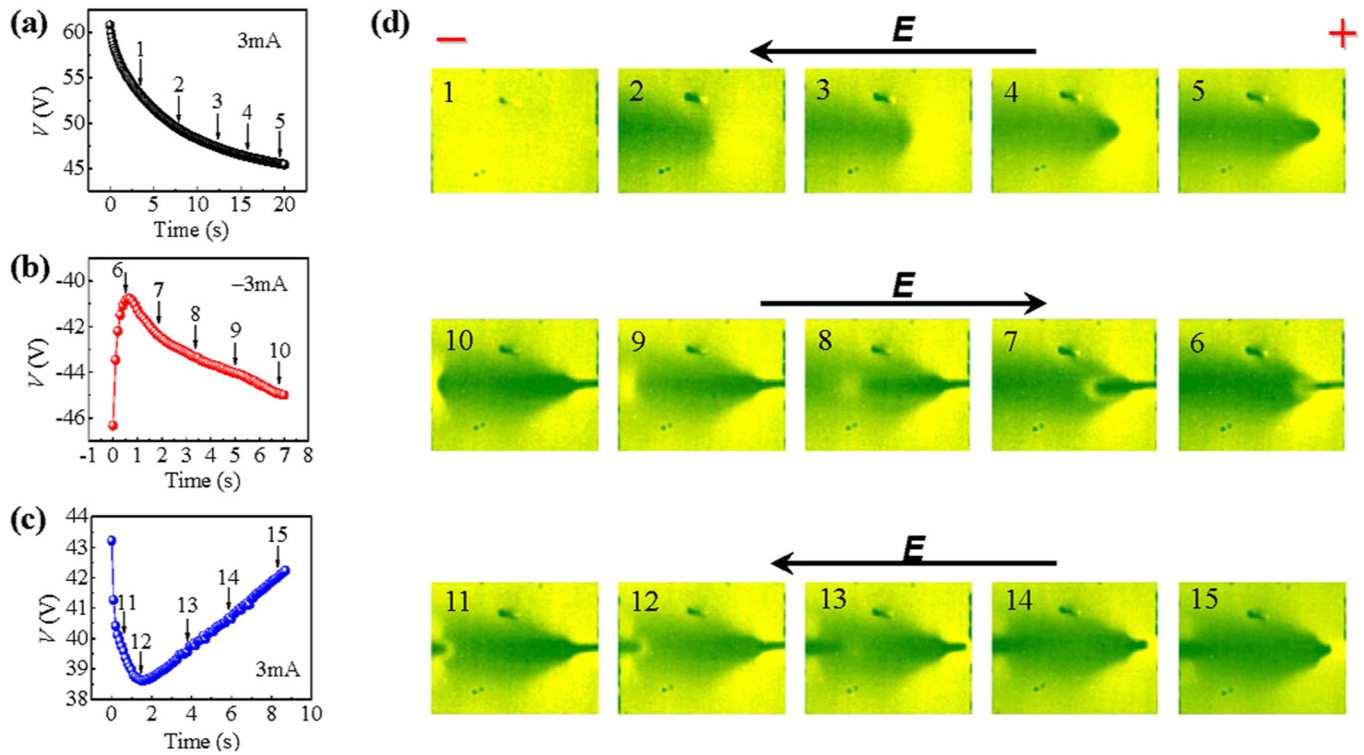


FIG. 2. (Color online) Time dependent voltage change of the planar device triggered by constant current (a) 3 mA, and then (b) -3 mA, and then (c) 3 mA. (d) Corresponding photo images, snapped at the states with the number from 1 to 15. The arrows correspond to the polarity direction of the applied electric voltage. For clarity, the color change was magnified digitally by subtracting the image of the non-conductive channel region from the image and then colored.

Each resistance states show the Ohmic I - V characteristics, meaning that no interfacial barrier exists in our sample. The RS polarity of the planar device should be originated from the asymmetric distribution of the electric field in the film due to the initial formation of the parabolic channel.

An interesting feature we should note during the low-to-high RS is that the device voltage always decreased firstly and then increased. That means the low-to-high RS is not a simply monotonic process and dependent on the application time of the constant current. To explain this feature, we recorded the photo image at A, B, C, and D four typical states, as shown in Fig. 3(c). For clarity further, the photo images were digitally colorized with color scale from blue to red indicating qualitatively the conductivity changes from high to low. At the state A, we found that the low resistance state was caused by the connection of the left parabolic channel with the bar-like channel protruded from the right electrode. However, a relatively low conductive region still existed between the two conductive channels (arrowed in Fig. 3(c)). At the state B, the bar-like channel was pushed forward further into the left channel, and the whole channel connection became better, especially forming an “arc-like” indirect connection at the circumference of the center. But the relatively low conductive region still existed in the channel center (arrowed in Fig. 3(c)). Surprisingly, at the state C when applying the reverse voltage, the low conductive regions at the channel center disappeared firstly, but the whole channel was still connected. That means the channel connection did not damaged but became better. These geometrical features explain why the sample resistance decreased at the beginning time of low-to-high RS process.

At the state D, the disconnection of the channel starts to appear at the right electrode side. Then, the disconnection distance became larger with time, resulting in the sample resistance increasing with time. The whole connection/disconnection processes are shown as a movie in Movie S1 in the supplementary materials.²⁹

When a higher constant current 5 mA was used to trigger the sample, we found that the RS behavior became instable. As shown in Fig. 4(a), both the high and the low resistance values increased with the switching number. After several switching cycles, a sudden drop of resistance would occur. From the photo images, we can see that the occurring position of the bar-like channel was different in each switching cycle. With the device resistance increasing, the bar-like channel shifted gradually from the electrode middle toward one of the electrode edges. That geometrically means the length of the conductive channel was prolonged. Since the device resistance was dominated by the conductive channel, the channel prolongation caused the resistance increase. When the bar-like channel reached the edge of the electrode, it shifted to the middle of the electrode again. Correspondingly, an abrupt decrease of device resistance took place. These images clearly show that the instable RS behavior is caused by the change of bar-like channel occurring position, which is unfixed under high external electric-field. These geometrical features should be helpful to give some insight into the improvement of RS-related device performance. For example, we can moderate the applied electric-field for inhibiting the instable RS. Moreover, we can design the geometrical shape of the device, which would change the electric-field distribution in the devices, to constrain the

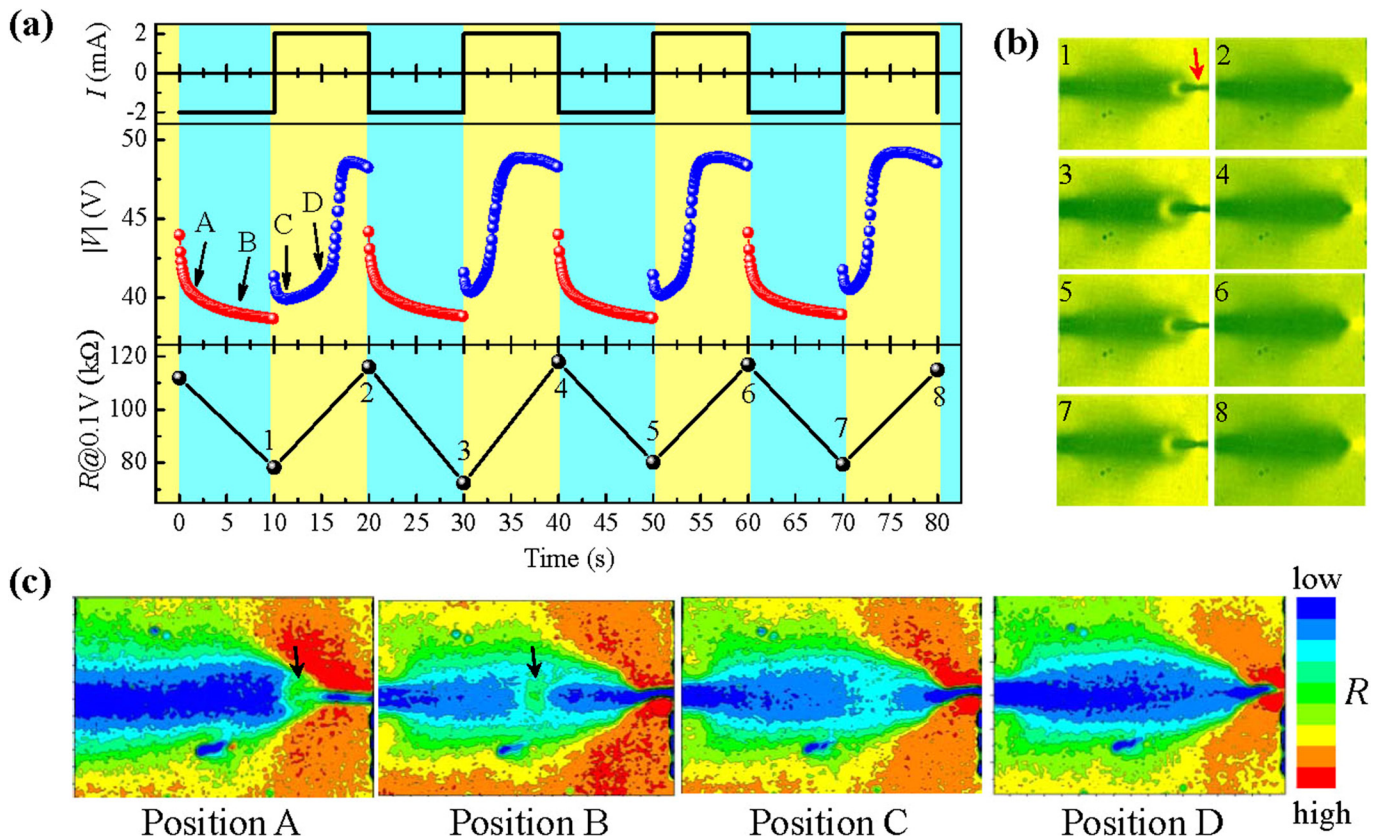


FIG. 3. (Color online) (a) Time dependent voltage change stressed by the constant current with amplitude alternated between -2 mA and 2 mA. The device resistance R was measured at the interval of constant current alternation at 0.1 V. (b) Corresponding photo images, snapped simultaneously with resistance measurement. (c) Multicolor mapping of the photo images snapped at the time of A, B, C, and D states shown in (a).

movement of channel occurring position. We note that the geometry influence on the performance has been demonstrated in the memristive nano-devices recently.²⁴

Now, we discuss the physical origin of the conductive channel. It has been demonstrated that the color change of tungsten oxide is due to the ion injection.²² Then, which ion was injected into the film during the color change? The color and resistance change phenomenon of the sample grown on the glass substrate was also found under high vacuum condition ($< 1 \times 10^{-5}$ Torr), indicating the independence of environmental condition. By the EDS analysis of the films grown on the glass substrate, we found that Na, Ca, Si, and Mg elements

besides W and O appeared in both the channel and other place, as shown in Fig. S2 and Table S1 in the supplementary materials.²⁹ These elements should generate from both the film and the glass substrate because the film thickness has only 400 nm while the EDS can detect nearly $1 \mu\text{m}$ thickness. By comparing Na content with other elements, we found that the Na content at the conductive channel region, especially at the breakdown region, is higher than at other places. We also tried the samples with other insulator substrates, such as quartz (SiO_2) and LaAlO_3 single crystal. Surprisingly, no RS behavior as well as the color change phenomenon can be observed. Based on these results, we suggest that Na^+ in the glass substrate would be

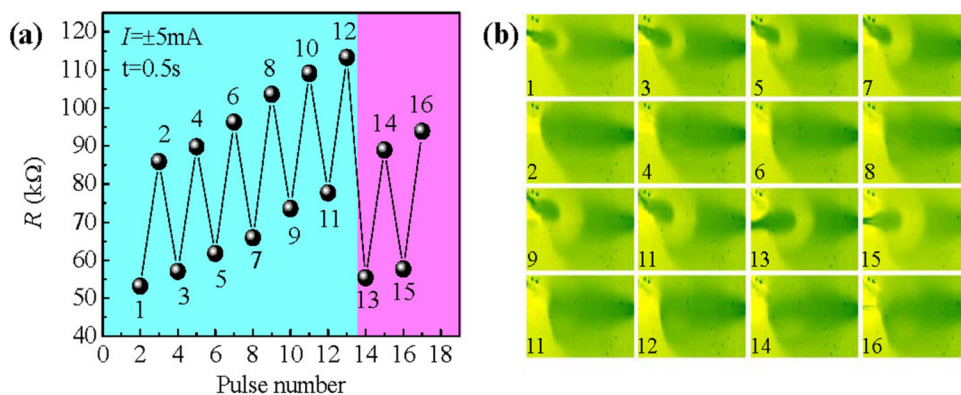


FIG. 4. (Color online) (a) Resistance switching triggered by constant current 5 mA with different polarity for 0.5 s. The measuring voltage is 0.1 V. (b) Corresponding photo images, snapped simultaneously with resistance measurement.

injected into the tungsten oxide films under the electric-field and resulting in the RS and color change of the film.

In our experiment, the threshold currents required for the conductive channel formation are different for the planar devices with different initial resistance values. As shown in Fig. 5, the threshold currents show a linear dependence with a slope of 0.5 on the initial resistance values in logarithmic plot. If we calculate the electric power by I^2R , the lowest powers are almost constant and about 0.3 W. **That means the main factor determining the conductive channel formation is not the applied current or voltage, but the electric power.** Thus, electrothermal effect should play a dominant role in the conductive channel formation. Let us assume the sample to be a heat source (see Fig. S3 in the supplementary materials²⁹). According to the thermal conductivity $k=0.75 \text{ W m}^{-1} \text{ K}^{-1}$ of the glass substrate we used and the device size $2a=300 \text{ nm}$, where a is half distance between two electrodes, it can be roughly calculated according to the function $\Delta T=p/\pi ka$, that the substrate temperature should be increased with the ΔT of about 850 K when the electric power $p=0.3 \text{ W}$ was exerted on the planar device.²¹ Considering the heat loss through the metal electrode, which can be seen as a heat sink due to its high thermal conductivity, the real temperature change should be lower than the calculated value. Based on these results, a scenario for the conductive channel formation can be drawn. Under the electric field, the temperature of the glass substrate increased due to the electrothermal effect. The high temperature causes the reaction between the tungsten oxide film and glass substrate at the interface, resulting in Na^+ diffusion into the tungsten oxide film. Then Na^+ migrated driven by the electric field to the cathode to form a sodium tungsten bronze region, which has higher conductivity and different colors. This process also explained why we could not observe the gradual growth of the initial parabolic channel from the anode but observe the dark region firstly in the device center region, where the temperature might be higher than other places due to the electric-field distribution (No. 1 and 2 images in Fig. 2(d)).

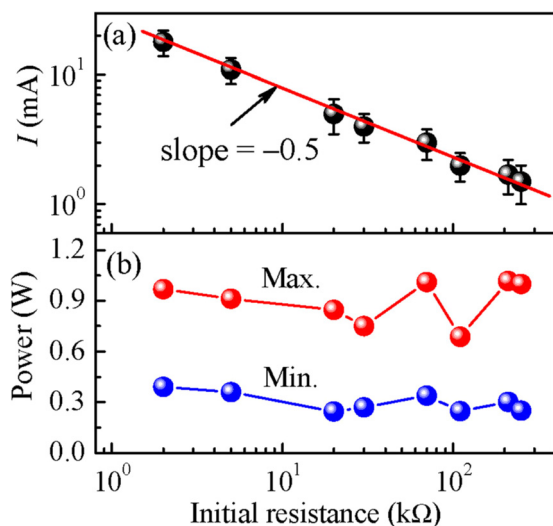


FIG. 5. (Color online) Dependence of (a) currents required for the conductive channel formation and (b) calculated electric power, $W=I^2R$, on the initial resistance of the planar device.

Figure 6 shows the micro-Raman spectra in the conductive channel and elsewhere. As can be seen, both the Raman spectra at region A and B show three intense bands at 270, 705, and 810 cm^{-1} , which are in good agreement with the characteristics of monoclinic WO_3 .²⁵ In the conductive channel region C, these bands become broad, meaning that the symmetry of crystal structure increased. This trend of crystal structure change is consistent with that of sodium tungsten bronze with increasing sodium content.²³ Similar change in Raman spectra has also been observed in lithium tungsten bronze with increasing lithium concentration.²⁶ Nevertheless, more experimental evidences are still needed to confirm the above assumption.

Note that this interesting bipolar switching behavior, observed in the planar sandwich device, involves only sodium ion movement in the tungsten oxide during the whole RS process, in contrast with previous studies typically involving electrochemical metallization, where the conductive channel generated by reduction and electrocrystallization of metal ions (e.g., Cu^+ , Ag^+).^{8,12,13,17} Even though sodium ion is not supposed to be involved in any semiconductor memory devices, the channel evolution processes should also be suitable to other ions, such as proton and lithium ions in tungsten oxide. These features also suggest an application of electric-field-induced cation (e.g., H^+ , Li^+ , Na^+) migration in transition metal oxides in the construction of electrical/optical-coupled reversible switching and data storage devices.^{27,28} On the other hand, the results of these preliminary investigations of the planar sandwich device, at present, leave open questions about the nature of the exact mechanisms of the process involved, such as the mechanism of the conductive channel shape, the "arc-like" connection, and non-monotonic disconnection during the RS process, which should be involved with the evolution of electric-field distribution with the ion movement and thermal distribution in the planar device. These aspects, as well as the influence of geometric shape and peripheral roughness of the electrodes on the channel evolution with downscaling of device size, need to be further investigated.

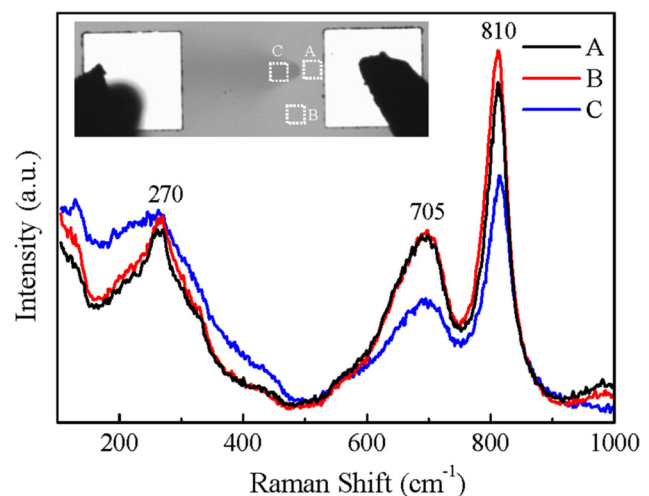


FIG. 6. (Color online) Raman spectra of the planar device. Inset shows the photo image of the planar device. The measured areas are noted by A, B, and C.

IV. CONCLUSION

In summary, the evolution of the conductive channel in Au/WO_{3-x}/Au planar devices was successfully visualized by the *in situ* optical image technique based on the color-conductivity dependence of tungsten oxide. Two types of conductive channels with parabolic and bar-like shapes were found in this planar device during RS processes. The “arc-like” indirect connection and non-monotonic disconnection between the two types of channels constructed the RS behavior in the planar device. The RS polarity was originated from the asymmetric shape of the two channels, which caused the asymmetric electric-field distribution in the device. The RS instability was caused by the change of the bar-like channel occurring position stressed by high external electric-field. The conductive channel formation is a thermal assisted process. In this process, sodium tungsten bronze formed by the sodium ion immersion into the film and then migration driven by the electric-field. These results will give some insight into the RS property improvement and mechanism elucidation and a possibility to develop electric/optical-coupled switch and data storage devices.

ACKNOWLEDGMENTS

This work was supported by the National Basic Research of China, the National Natural Science Foundation of China, the Knowledge Innovation Project of the Chinese Academy of Sciences, and the Beijing Municipal Nature Science Foundation.

- ¹G. I. Meijer, *Science* **319**, 1625 (2008).
- ²Y. Fujisaki, *Jpn. J. Appl. Phys.* **49**, 100001 (2010).
- ³G. S. Kreyнина, *Radio Eng. Electro. Phys.* **7**, 1949 (1962).
- ⁴T. W. Hickmott, *J. Appl. Phys.* **33**, 2669 (1962).
- ⁵S. Q. Liu, N. J. Wu, and A. Ignatiev, *Appl. Phys. Lett.* **76**, 2749 (2000); A. Beck, J. G. Bednorz, Ch. Gerber, C. Rossel, and D. Widmer, *ibid.* **77**, 139 (2000).
- ⁶R. Oligschlaeger, R. Waser, R. Meyer, S. Karthäuser, and R. Dittmann, *Appl. Phys. Lett.* **88**, 042901 (2006); M. Hamaguchi, K. Aoyama, S. Asanuma, Y. Uesu, and T. Katsufuji, *ibid.* **88**, 142508 (2006); D. S. Shang, J. R. Sun, L. Shi, and B. G. Shen, *ibid.* **93**, 102106 (2008).
- ⁷S. Seo, M. J. Lee, D. H. Seo, E. J. Jeoung, D. S. Suh, T. S. Joung, I. K. Yoo, I. R. Hwang, S. H. Kim, I. S. Byun, J. S. Kim, J. S. Choi, and B. H. Park, *Appl. Phys. Lett.* **85**, 5655 (2004); C. Rohde, B. J. Choi, D. S. Jeong, S. Choi, J. S. Zhao, and C. S. Hwang, *ibid.* **86**, 262907 (2005); R. Dong, D. S. Lee, W. F. Xiang, S. J. Oh, D. J. Seong, S. H. Heo, H. J. Choi, M. J. Kwon, S. N. Seo, M. B. Pyun, M. Hasan, and H. Hwang, *ibid.* **90**, 042107 (2007); D. S. Shang, L. Shi, J. R. Sun, B. G. Shen, F. Zhuge, F.; R. W. Li, and Y. G. Zhao, *ibid.* **96**, 072103 (2010).
- ⁸T. Sakamoto, H. Sunamura, H. Kawaura, T. Hasegawa, T. Nakayama, and M. Aono, *Appl. Phys. Lett.* **82**, 3032 (2003); C. Schindler, S. C. Puther Thermadam, R. Waser, and M. N. Kozicki, *IEEE Trans. Electron. Dev.* **54**, 2762 (2007); M. N. Kozicki, M. Park, and M. Mitkova, *IEEE Trans. Nanotechnol.* **4**, 331 (2005).
- ⁹D. B. Strukov, G. S. Snider, D. R. Stewart, and R. S. Williams, *Nature* **453**, 80 (2008).
- ¹⁰J. Borghetti, G. S. Snider, P. J. Kuekes, J. J. Yang, D. R. Stewart, and R. S. Williams, *Nature* **464**, 873 (2010).
- ¹¹S. H. Jo, T. Chang, I. Ebong, B. B. Bhadviya, P. Mazumder, and W. Lu, *Nano Lett.* **10**, 1297 (2010); T. Ohno, T. Hasegawa, T. Tsuruoka, K. Terabe, J. K. Gimzewski, and M. Aono, *Nature Mater.* **10**, 591 (2011).
- ¹²R. Waser, R. Dittmann, G. Staikov, and K. Szot, *Adv. Mater.* **21**, 2632 (2009).
- ¹³R. Waser and M. Aono, *Nature Mater.* **6**, 833 (2007).
- ¹⁴B. J. Choi, D. S. Jeong, S. K. Kim, C. Rohde, S. Choi, J. H. Oh, H. J. Kim, C. S. Hwang, K. Szot, R. Waser, B. Reichenberg, and S. J. Tiedke, *J. Appl. Phys.* **98**, 033715 (2005).
- ¹⁵K. Szot, W. Speier, G. Bihlmayer, and R. Waser, *Nature Mater.* **5**, 312 (2006).
- ¹⁶M. Janousch, G. I. Meijer, U. Staub, B. Delley, S. F. Karg, and B. P. Andreasson, *Adv. Mater.* **19**, 2232 (2007).
- ¹⁷X. Guo, C. Schindler, S. Menzel, and R. Waser, *Appl. Phys. Lett.* **91**, 133513 (2007); C. P. Hsiung, H. W. Liao, J. Y. Gan, T. B. Wu, J. C. Hwang, F. Chen, and M. J. Tsai, *ACS Nano* **4**, 5414 (2010).
- ¹⁸R. Yasuhara, K. Fujiwara, K. Horiba, H. Kumigashira, M. Kotsugi, M. Oshima, and H. Takagi, *Appl. Phys. Lett.* **95**, 012110 (2009).
- ¹⁹Y. C. Yang, F. Pan, Q. Liu, M. Liu, and F. Zeng, *Nano Lett.* **9**, 1636 (2009).
- ²⁰Z. Xu, Y. Bando, W. Wang, X. Bai, and D. Golberg, *ACS Nano* **4**, 2515 (2010); D. H. Kwon, K. M. Kim, J. H. Jang, J. M. Jeon, M. H. Lee, G. H. Kim, X. S. Li, G. S. Park, B. Lee, S. Han, M. Kim, and C. S. Hwang, *Nat. Nanotechnol.* **5**, 148 (2010).
- ²¹K. Azumi, K. Aoyama, S. Asanuma, Y. Uesu, and T. Katsufuji, *Phys. Rev. B* **79**, 121101 (2009).
- ²²G. A. Niklasson and C. G. Granqvist, *J. Mater. Chem.* **17**, 127 (2007).
- ²³S. Raj, H. Matsui, S. Souma, T. Sato, T. Takahashi, A. Chakraborty, D. D. Sarma, P. Mahadevan, S. Oishi, W. H. McCarroll, and M. Greenblatt, *Phys. Rev. B* **75**, 155116 (2007).
- ²⁴Q. F. Xia, M. D. Pickett, J. J. Yang, M. X. Zhang, J. Borghetti, X. M. Li, W. Wu, G. M. Ribeiro, and R. S. Williams, *Nanotechnology*, **22**, 254026 (2011).
- ²⁵P. Tägtström and U. Jansson, *Thin Solid Films* **35**, 107 (1999).
- ²⁶S. H. Lee, M. J. Seong, H. M. Cheong, E. Ozkan, E. C. Tracy, and S. K. Deb, *Solid State Ionics* **156**, 447 (2003).
- ²⁷W. T. Wu, J. J. Wu, and J. S. Chen, *ACS Appl. Mater. Interfaces* **3**, 2616 (2011).
- ²⁸A. Moradpour, O. Schneegans, S. Franger, A. Revcolevschi, R. Salot, P. Auban-Senzier, C. Pasquier, E. Svoukis, J. Giapintzakis, O. Dragos, V. C. Ciomaga, and P. Chrétien, *Adv. Mater.* **23**, 4141 (2011).
- ²⁹See supplementary material at <http://dx.doi.org/10.1063/1.3691204> for figures and table of bipolar RS with opposite polarity (Fig. S1), material analysis of WO_{3-x} film on the glass substrate by EDS spectra (Fig S2 and Table S1), and schematic picture of the diffusion of the heat produced by electric power (Fig. S3); movies of the bipolar stable RS (Movie S1) and instable RS (Movie S2).